


Porous monoliths consisting of aluminum oxyhydroxide nanofibrils: 3D structure, chemical composition, and phase transformations in the temperature range 25–1700 °C

A. Khodan  · T. H. N. Nguyen · M. Esaulkov ·
M. R. Kiselev · M. Amamra · J.-L. Vignes · A. Kanaev

Received: 13 January 2018 / Accepted: 27 June 2018 / Published online: 15 July 2018
© Springer Nature B.V. 2018

Abstract We present a study on the chemical and structural transformations in highly porous monolithic materials consisting of the nanofibrils of aluminum oxyhydroxides (NOA, $\text{Al}_2\text{O}_3 \cdot n\text{H}_2\text{O}$) in the temperature range 20–1700 °C. A remarkable property of the NOA material is the preservation of the monolithic state during annealing over the entire temperature range, although the density of the monolith increases from ~ 0.02 up to ~ 3 g/cm³, the total porosity decreases from 99.3 to 25% and remains open up to 4 h annealing at the temperature ~ 1300 °C. The physical parameters of NOA monoliths such as density, porosity, specific area were studied and a simple physical model describing these parameters as the function of the average size of NOA fibrils—the basic element of 3D structure—was proposed. The observed thermally induced changes in composition and structure of NOA were successfully described and two mechanisms of mass transport in NOA materials were revealed. (i) At moderate temperatures ($T \leq 800$ °C), the mass transport occurs along a surface of amorphous single fibril, which

results in a weak decrease of the length-to-diameter aspect ratio from the initial value ~ 24 till ~ 20 ; the corresponding NOA porosity change is also small: from initial ~ 99.5 to 98.5%. (ii) At high temperatures ($T > 800$ °C), the mass transport occurs in the volume of fibrils, that results in changes of fibrils shape to elliptical and strong decrease of the aspect ratio down to ≤ 2 ; the porosity of NOA decreases to 25%. These two regimes are characterized by activation energies of 28 and 61 kJ/mol respectively, and the transition temperature corresponds to the beginning of γ -phase crystallization at 870 °C.

Keywords Nanomaterials · Mesoporous materials · Aerogel · Aluminum oxyhydroxides · Alumina · 3D nanostructure · Phase transitions · Structural water · Modeling and simulation

Introduction

The oxidation of liquid-metal alloys resulting in the formation of porous oxides has been discovered in Al-Hg system over a century ago (Wislicenus 1908). Since that time, different ways of obtaining aerogels consisting of nanofibrous alumina organized in 2D and 3D nanostructures have been proposed and investigated (Noordin and Liew 2010). Among the various methods for preparing aerogels, the growth of porous NOA monolith on the surface of the liquid metal alloys has considerable advantage because it provides 3D nanomaterials preparation with highly reproducible chemical and physical properties. Further development of this technique results in the

A. Khodan (✉) · M. R. Kiselev
A.N. Frumkin Institute of Physical Chemistry and
Electrochemistry RAS (IPCE RAS), 199071 Moscow, Russia
e-mail: anatole.khodan@gmail.com

T. H. N. Nguyen · M. Amamra · J.-L. Vignes · A. Kanaev
Laboratoire des Sciences des Procédés et des Matériaux, CNRS,
Université Paris 13, Sorbonne Paris Cité, 93430 Villetaneuse,
France

M. Esaulkov
Institute on Laser and Informational Technologies, Russian
Academy of Sciences, 140700 Moscow, Russia

laboratory technology for the synthesis of nanofibrous amorphous alumina grown on deoxidized metallic aluminum plates wetted by mercury upon exposure of humid air (Pinnel and Bennett 1972). This method has been improved by doping a mercury amalgam with silver, which permitted better control of growth rate of NOA monolith and provide high homogeneity of the samples grown. The raw NOA monoliths obtained in this way can be annealed to obtain oxide materials with a given porosity, density, and specific surface area (Vignes et al. 1997; Di Costanzo et al. 2004; Vignes et al. 2008). It was shown that annealing of NOA materials does not affect their integrity and porous structure, leading only to an isotropic decrease only in the linear dimensions of the samples. At the temperature range ~ 25 – 1700 °C, the structural transformations were observed in NOA materials—from amorphous state to γ -, θ -, and α -aluminas (Vignes et al. 1997; Di Costanzo et al. 2004; Vignes et al. 2008; Askhadullin et al. 2008). The corresponding characteristics of the NOA samples also are changing: the density increased from 0.02 to ~ 3 g/cm³; porosity and specific surface area decreasing from 99.3 to 25% and from ~ 300 m²/g till 1 m²/g respectively. It should also be noted that a similar method of making porous oxides was proposed recently, which is based on the use of different of liquid alloys: Ga-Al and Bi-Al (Askhadullin et al. 2008; Bouslama et al. 2011).

Thermally treated NOA samples were used to create new oxide nanocomposites, functional nanomaterials, and hybrid structures (Bouslama et al. 2011; Asadchikov et al. 2015; Bouslama et al. 2012; Mukhin et al. 2012; Stepanenko O et al. 2015). In particular, potential applications of NOA materials in catalysis (Asadchikov et al. 2015; Bouslama et al. 2012) and THz optics (Mukhin et al. 2012; Stepanenko et al. 2015) have been demonstrated and discussed. In the same time, an adequate theoretical model describing the morphological changes, structural, and phase transformations in NOA materials has not been proposed until now.

The present report proposes a physical model that describes quantitatively the morphological changes of NOA induced by the diffusion transport, chemical, and phase transformations in the temperature range between 20 and 1700 °C. Experimental results obtained in this study are discussed along with the data reported earlier. Within the proposed model, it is shown that the changes in the physical properties of NOA can be described as the evolution of the key structural element—an average fibril and its aspect ratio (length/diameter).

Experimental

The samples of NOA monoliths were grown in the chamber filled with an atmospheric air with a humidity ~ 70 – 80% at room temperature ~ 25 °C. The primary layers with the aerosol structure are formed as a result of the oxidation reaction of the surface of a mercury-silver liquid solution deposited as a thin layer on a foil 99.9% aluminum. Under these conditions, a monolithic sample of NOA is growing with the rate of ~ 1 cm/h (Vignes et al. 2008), Fig. 1a.

Complex studies of morphological and structural features of the NOA samples have been carried out using powder X-ray diffraction (INEL XRG 3000 and Bruker D8 Advance diffractometers with X-ray source Cu-K α ($\lambda = 1.5418$ Å), transmission electron microscopy (JEOL2011 equipped with 200 keV LaB₆ gun), and scanning electron microscopy (Zeiss Supra 40 VP SEM-FEG operated at low acceleration voltage). Neutron scattering studies were carried out using small-angle KWS-2 and ultra-small-angle KWS-3 diffractometers in Research Neutron Source Heinz Maier-Leibnitz, reactor FRM II (Khodan et al. 2018).

The specific surface area and pore size distribution were determined by low-temperature nitrogen adsorption using a Coulter SA3100 and QuantaChrome Nova 4200B analyzers. Before the measurements, the samples were degassed in vacuum at 120 °C for 16 h. Specific surface area was calculated using the Brunauer-Emmett-Teller (BET) model.

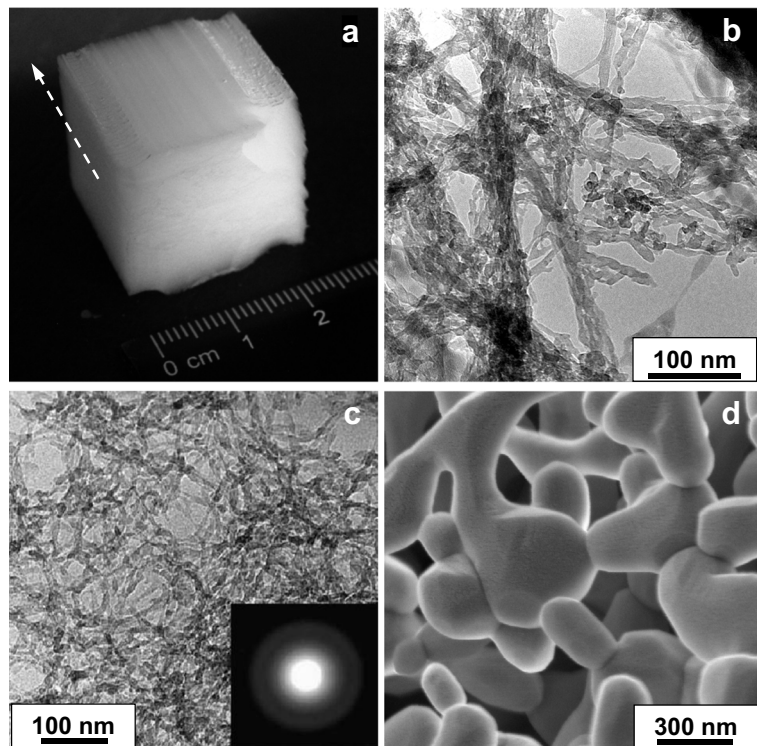
The thermogravimetric (TG) analysis and differential scanning calorimetry (DSC) studies were performed using the SETARAM TG92 and Intertech TGA Q500 equipment. The sample with mass about 20 mg was heated in argon flow (~ 50 ml/min) at the increment rates between 0.1 and 50 °C/min up to the maximum temperature of 1000 °C.

Results and discussion

Effect of annealing on the structure and chemical composition of NOA

The characteristic structure of raw NOA is filamentary-nodular that is clearly visible on TEM images (Fig. 1b). The monolithic structure of NOA is formed by entangled fibrils of hydrated alumina possessing an average diameter of ~ 4 – 10 nm and length within 150–

Fig. 1 **a** View of raw NOA sample, the direction of growth is indicated by arrow. **b** TEM image of the raw NOA sample. **c** TEM image of NOA sample annealed at 400 °C (Vignes et al. 2008). **d** SEM image of NOA sample annealed during 4 h at 1300 °C (Di Costanzo et al. 2004)



300 nm. The chemical and phase composition of raw NOA can be described as an amorphous hydrated aluminum oxyhydroxide with water content of 40–43 wt.%, having very high porosity $\geq 99\%$, and specific surface area about 250–300 m²/g; the latter can be increased two times or more by applying a freeze drying.

Thermal treatment of raw NOA at temperatures below 800 °C does not affect significantly an amorphous structure, while at 1150 °C and higher the initial structure of fibrils begins to change, what is accompanied by a significant reducing of the specific surface area and the volume of mesopores. Crystallization and subsequent phase transitions to γ -, θ -, and α -alumina takes place in NOA samples under 4 h isochronous annealing at 870, 1100, and 1200 °C respectively (Table 1). The characteristic diameter of the fibrils and the corresponding values of specific surface area of polymorphs are 7 nm and 150 m²/g for γ -alumina, 10 nm and 100 m²/g for θ -alumina, and 250 nm and 10 m²/g for α alumina phases. Raw NOA possesses a very low mass density ~ 0.025 g/cm³ which increases up to 3 g/cm³ at 1700 °C—the maximum treatment temperature applied. As shown at SEM image of the sample treated at 1300 °C (Fig. 1d), the fibrils are transformed to well-crystallized α -Al₂O₃

particles. The respective size of ellipsoidal particles varies from 150 to 250 nm with the average value of ~ 200 nm.

Chemical and structural transformations The XRD patterns of NOA treated at different temperatures are shown in Fig. 2. Up to ~ 650 °C, they do not reveal any significant change in the amorphous structure. Our experimental data and those of previous studies (Vignes et al. 1997; Di Costanzo et al. 2004; Vignes et al. 2008) show that the fibrils passes four structural transitions upon isochronous annealing in the temperature range 800–1600 °C going from the native amorphous state, consisting of chains of Al³⁺ cations in the octahedral surrounding of anions (Frappart 2000), to the stable α -crystalline state as summarized in Table 1. Aluminum oxyhydroxides obtained by the chemical precipitation are also included in this table for comparison.

We noticed that the very beginning of γ -Al₂O₃ crystallization from the amorphous alumina obtained by chemical precipitation can be detected at temperatures as low as ~ 400 °C (see Table 1), which follows from our detailed analysis of electron diffraction patterns. The crystallization is a kinetically limited process and its rate is extremely low in this range of temperatures.

Table 1 Structural and phase transitions in aluminum oxyhydroxides

Phase transition		T , °C		
		NOA ^a	Oxyhydroxides ^b (chemical precipitation)	
			Onset	Completed
I-II	Mixed state: hydrated amorphous alumina with water	≤ 100	–	–
II	Amorphous structure, partially dehydrated	~ 450	–	–
II-III	Amorphous $\rightarrow \gamma\text{-Al}_2\text{O}_3$	870	320–450	600–700
III-IV	$\gamma\text{-Al}_2\text{O}_3 \rightarrow \theta\text{-Al}_2\text{O}_3$	1000	830–950	1050
IV-V	$\theta\text{-Al}_2\text{O}_3 \rightarrow \alpha\text{-Al}_2\text{O}_3$	1200	1050	1100

^a Isochronous annealing during 4 h (Frappart 2000)

^b Ref. (McHale et al. 1997a, b)

Moreover, crystallization of single (non-aggregated) nanofibrils can be delayed to higher temperatures due to a contribution of surface energy, in agreement with previous observations in oxide nanoparticles (Zhang and Banfield 1998). In particular, an assessment of the enthalpy of formation for $\gamma\text{-Al}_2\text{O}_3$ with the surface area exceeding $\sim 125 \text{ m}^2/\text{g}$ predicts its decreasing lower compared to that of $\alpha\text{-Al}_2\text{O}_3$ (Frappart 2000; Navrotsky 2003). This effect also concerns crystallization from the amorphous phase (Khatim et al. 2013). Amorphous fibrils begins to crystallize at a temperature above $870 \text{ }^\circ\text{C}$ what is in agreement with the results published earlier (Vignes et al. 2008; Frappart 2000). An additional confirmation of the dominant contribution of surface transport to the kinetics of crystallization can be a significant slowdown of γ -, θ -, and α -alumina phase transformation in NOA materials, when the surface of fibrils are covered with a few monolayers of silica (Di Costanzo et al. 2004). It should be noted that silica layer also prevents the elimination of the structural water from NOA what inhibits the phase transformation. Under the 4 h isochronous annealing, the overall effect appears as a “phase transition temperature shift up” within $\sim 150\text{--}300 \text{ }^\circ\text{C}$ (Table 1).

Key changes in the chemical composition of NOA upon annealing are related to the losses of the adsorbed and structural water. Results of TG measurements in the temperature range of $25\text{--}950 \text{ }^\circ\text{C}$ are presented at Fig. 3 as the relative mass losses and related water content in

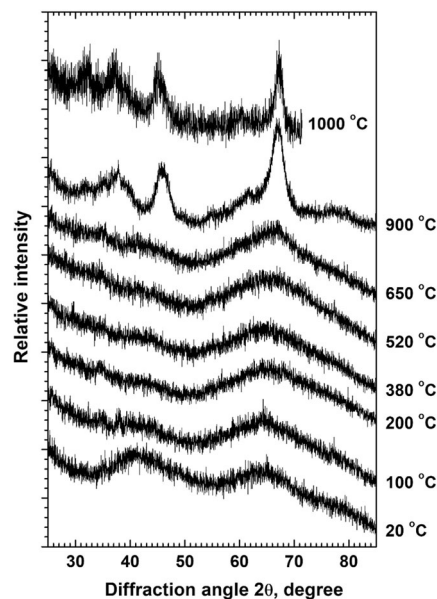


Fig. 2 XRD patterns obtained from NOA samples after isochronous 4 h annealing in air at different temperatures

raw and thermally treated NOA samples. At the given temperature $T \text{ }^\circ\text{C}$, we can present a relative molecular composition $n(T)$ as the sum of the two types of water state:

$$n(T) = n_{str}(T) + n_{ads}(T) \quad (1)$$

where $n_{str}(T)$ and $n_{ads}(T)$ are the relative fractions of the structural water ($\text{Al}_2\text{O}_3 \cdot n_{str} \text{H}_2\text{O}$) and the adsorbed water at the NOA surface. With an aim to separate and define $n_{str}(T)$ and $n_{ads}(T)$ values, the studies were performed using two groups of samples. For the first group of samples, a weight loss was measured in relation to the initial raw state of NOA; the samples of second group passed preliminary annealing at the temperature $T_p = 100; 380; 400; 520; 660 \text{ }^\circ\text{C}$ during 4 h and were measured after cooling down to room temperature in air (Fig. 3).

From the TG results, it follows that the raw NOA contains about 3.6 water molecules per Al_2O_3 , which exceeds the water content in the stoichiometric hydroxide. This confirms that the raw NOA fibrils consist of aluminum oxyhydrates with excess of adsorbed molecular water. The loss of structural water $n_{str}(T)$ starts below $400 \text{ }^\circ\text{C}$ and is accompanied with partial dehydration of the amorphous aluminum oxyhydroxide. Stable compositions $\text{Al}_2\text{O}_3 \cdot 1.5\text{H}_2\text{O}$ and $\text{Al}_2\text{O}_3 \cdot 0.9\text{H}_2\text{O}$ are formed at ~ 100 and $380 \text{ }^\circ\text{C}$ respectively. The last composition can be interpreted as amorphous phase of

partially dehydrated boehmite $\text{Al}_2\text{O}_3 \cdot \text{H}_2\text{O}$, that is in an agreement with the data on the beginning of $\gamma\text{-Al}_2\text{O}_3$ crystallization (see Table 1). The further increase in temperature up to 700 °C moderately affects the $\text{Al}_2\text{O}_3 \cdot x\text{H}_2\text{O}$ composition with x decreasing down to 0.4, which completes the formation of γ -phase at 870 °C in agreement with data presented by J-L. Vignes et al. 2008.

The values $n_{str}(T)$ and $n_{ads}(T)$ are plotted in Fig. 4 versus preannealing temperature T_p . The main changes in $n(T)$ are caused with the loss of water bound in NOA structure $n_{str}(T)$ and can be associated with hydroxide decomposition, whereas $n_{ads}(T)$ only weakly depend on the preliminary annealing temperature (Fig. 4). It should be noted the change in the properties of NOA adsorption surface at annealing temperatures $T \geq 400$ °C indicated by the arrow in Fig. 4a.

Analysis of the Table 2 data for the dependence of $n_{str}(T) = f(T_p)$ allowed to estimate the activation energy of oxyhydroxide decomposition ($E_D = 22 \pm 5$ kJ/mol using least square fit for Arrhenius equation:

$$\ln\left(\frac{n_0}{n_{str}(T_p)} - 1\right) = const - \frac{E_a}{k_B T_p} \quad (2)$$

where n_0 is the composition of raw NOA ($\text{Al}_2\text{O}_3 \cdot 3.6\text{H}_2\text{O}$), and k_B is the Boltzmann constant.

An increase in the annealing temperature activates the diffusive mass transport in NOA, which leads to the material densification due to morphological changes in nanofibrils and beginning of nucleation of new crystalline phases (Fig. 2). The annealing for 4 h at temperatures ranging from 100 to 1700 °C does not affect the

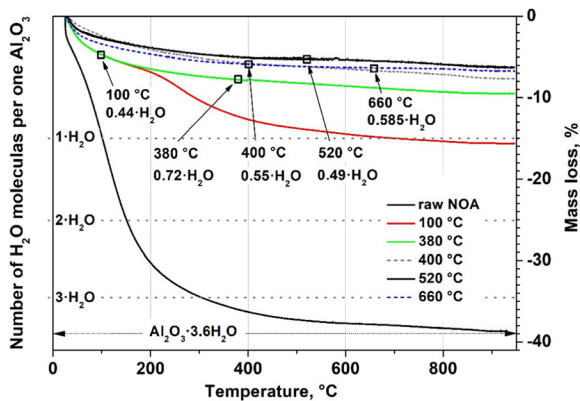


Fig. 3 Relative loss of water molecules per Al_2O_3 after annealing of NOA samples in air at different temperatures. All NOA samples were monolithic except the sample of powder NOA annealed at 660 °C

integrity of NOA samples while their dimensions decreases and mass density increases, as confirmed by the experimental data presented in Fig. 5a. However, below 450 °C, the mass density changes are negligible. This is related to the water desorption from NOA fibrils as explained in the previous discussion. Indeed, taking into account the water losses, (1) we evaluated the mass density of NOA fibrils as shown in Fig. 5b. The comparison between the measured and calculated mass densities indicates major surface water losses below 450 °C. Based on this result, we conclude that the fibril densification is continuous in the whole temperature range and its mechanism appreciably changes only at temperatures > 800 °C, when the mass transport mechanism changes from surface diffusion to sintering. These processes are quantitatively described in the framework of the 3D model proposed.

Intermediate metastable phases Five relatively stable phases can be identified in NOA upon annealing in the temperature range from 20 °C up to 1700 °C.

- (I) The NOA synthesized in ambient air with relative humidity $\sim 80\%$ at 25 °C has the chemical composition $\text{Al}_2\text{O}_3 \cdot n\text{H}_2\text{O}$ with $n \geq 3$. The NMR studies have shown that Al^{+3} cations have anionic surroundings including octahedral (83%), pentahedral (16%), and tetrahedral (1%) (Frappart 2000). Consequently, the NOA structure consists of polynuclear aqua-hydroxide complexes of aluminum cation and water molecules connected with hydrogen bonds in different spatial alignments.
- (II) The native structure of NOA starts losing water and decomposes when heated to moderate temperatures ~ 100 °C. It progressively transforms into an

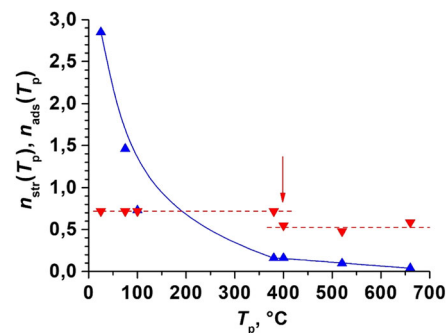


Fig. 4 Variation of the water molecular ratio per Al_2O_3 for structural (\blacktriangle) and adsorbed (\blacktriangledown) components in NOA samples with the temperature of pre annealing T_p (Table 2)

Table 2 Variation of molar ratio $\text{H}_2\text{O}/\text{Al}_2\text{O}_3$ for NOA samples with annealing temperature: $n_x = n_{str} + n_{ads}$

Molar ratio $\text{H}_2\text{O}/\text{Al}_2\text{O}_3$	The temperature of annealing x , °C						
	25	75	100	380	400	520	660
n_x , water total	3.57	2.18	1.45	0.88	0.71	0.58	0.62
n_{str} , structural water	2.85	1.46	0.73	0.16	0.16	0.096	0.038
n_{ads} , adsorbed water	0.72	0.72	0.72	0.72	0.55	0.48	0.59

amorphous oxide of $\text{Al}_2\text{O}_3 \cdot n\text{H}_2\text{O}$ composition with $n \leq 1.5$. A further increase in temperature does not promote significant changes in the amorphous structure, while the structural water content continuously reduces until $n \approx 0.1$ at 450–500 °C.

(III) At ~ 450 °C, the crystallization into $\gamma\text{-Al}_2\text{O}_3$ phase begin, which preserves a small amount of structural water $n < 0.1$. This small amount of water is necessary for stabilization of the transition phase (McHale et al. 1997a, b). However, the

crystallization in nanofibrous alumina is delayed to 870 °C (Vignes et al. 1997), and NOA monoliths remains amorphous in the extended temperature range between 100 and 800 °C and converts to $\gamma\text{-Al}_2\text{O}_3$ at 870 °C.

(IV) After 4 h annealing at $T \geq 1000$ °C, $\gamma\text{-Al}_2\text{O}_3$ converts to $\theta\text{-Al}_2\text{O}_3$, which is accompanied by a further reduction of the structural water content to $n < 0.04$.

(V) The temperature increase to 1200 °C leads to the formation of well-crystallized stable $\alpha\text{-Al}_2\text{O}_3$ polymorph, which does not contain any appreciable amount of structural water. This phase transition is completed at 1250 °C with the annealing time of 4 h.

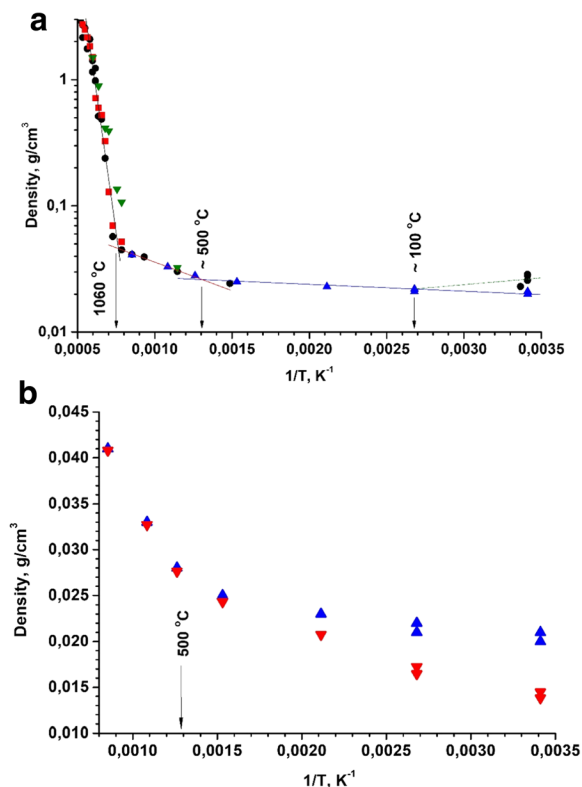


Fig. 5 **a** Density of NOA as a function of the annealing temperature (isochronous annealing time 4 h). The different series of measurements are indicated with different markers ●, ▼, and ▲. **b** Measured density of NOA (▲) and NOA density after correction for the water adsorbed at the surface (▼)

The main changes in chemical composition, phase structure, and morphology of the nanofibrils of NOA materials during annealing can be described in the framework of the physical model presented in the next chapter.

3D model of NOA materials

We assume that monolithic structure of NOA materials consist of entangled hydrated alumina fibrils with an average diameter d and length a (Figs. 1b–d). These fibrils form the porous structure as a network with multiple connections at the cross points. Upon annealing the aspect ratio a/d decreases and elementary fibrils progressively shorten and transform into ellipsoidal-shape particles, when the stable $\alpha\text{-Al}_2\text{O}_3$ polymorph is formed at temperatures above 1200 °C. Even in this case, the interconnected deformed fibrils can be recognized (Fig. 1d). Therefore, we relate the mass density and specific area of NOA materials to the evolution of the shape of elementary fibril. A relevant 3D geometrical model of the raw NOA material is presented in Fig. 6, where the primary volume a^3 contains n_f fibers

that interconnect arbitrary and are surrounded with a free volume V_p . The total volume of fibrils is $V_f = n_f \frac{\pi}{4} ad^2$ and their mass $M_f = n_f \cdot \rho_f \cdot \frac{\pi}{4} d^2 a$, where ρ_f is a specific density of the fibril's material. Corresponding specific surface area of M_f shall comply with $S_{sp} = n_f \cdot s_f \approx n \cdot \pi da$, where s_f is the surface of a single fibril. It is evident that M_f and S_{sp} depend on the aspect ratio a/d .

Mass density We estimated a specific density of the fibril's material close to $\rho_f = 2.4 \text{ g/cm}^3$. This reasonably agrees with the data for different crystalline oxyhydrates and aluminum oxides phases with different water content: 2.42 g/cm^3 for gibbsite $\text{Al}_2\text{O}_3 \cdot 3\text{H}_2\text{O}$, 2.53 g/cm^3 for bayerite $\text{Al}_2\text{O}_3 \cdot 3\text{H}_2\text{O}$, 3.01 g/cm^3 for boehmite $\text{Al}_2\text{O}_3 \cdot \text{H}_2\text{O}$, 3.5 and up to 3.9 g/cm^3 in $\gamma\text{-Al}_2\text{O}_3$ phase stabilized by the structural water. At temperatures below $1200 \text{ }^\circ\text{C}$, the maximum density 3.67 g/cm^3 can be obtained for $\gamma\text{-Al}_2\text{O}_3$, and 3.99 g/cm^3 for $\alpha\text{-Al}_2\text{O}_3$ phase at the high sintering temperatures $T > 1200 \text{ }^\circ\text{C}$.

The mass density of raw NOA material ρ_0 can be calculated as the mass of nanofibrils located in the volume a^3 :

$$\rho_0 = \frac{M_f}{a^3} = n_f \rho_f \cdot \frac{\pi}{4} \left(\frac{d_0}{a_0}\right)^2 \tag{3}$$

or an average number n of the fibrils in the volume a^3 can be estimated:

$$n_f = \frac{4 \rho_0}{\pi \rho_f} \left(\frac{a_0}{d_0}\right)^2 \tag{4}$$

Using measured mass density $\rho_0 \approx 0.025 \text{ g/cm}^3$ of raw NOA and aspect ratio variations a_0/d_0 between 4 and 16, the number of fibrils in the volume a^3 can be estimated: $n_f \approx 10 \pm 6$. We notice that the knowledge of

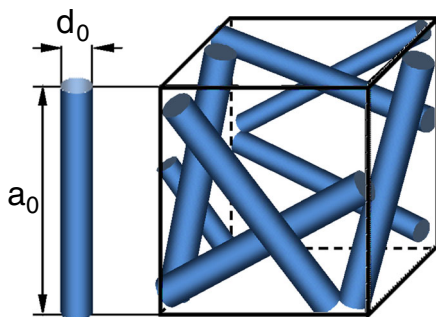


Fig. 6 3D presentation of NOA structural unit as a single pore with incorporated fibrils. The raw fibrils averaged diameter and length are respectively d_0 and a_0 and the aspect ratio is a_0/d_0

the true pore geometry is not necessary for calculation of the NOA-specific density with the rise of annealing temperature; the proposed model assumes that it scales with $\rho \propto (d/a)^2$.

Porosity and specific surface area The porosity of NOA can be determined as a fraction of the volume free from the nanofibrils. From the definitions for n_f and M_f follows:

$$P = 1 - \frac{V_f}{a^3} = 1 - \frac{M_f}{a^3 \cdot \rho_f} = 1 - \frac{n_f \pi}{4} \left(\frac{d}{a}\right)^2 \tag{5}$$

The total surface of all the nanofibrils located inside a primary volume a^3 can be presented as follows:

$$S_f = n_f \cdot s_f = n_f \cdot \pi da, \tag{6}$$

and specific surface area of raw NOA material can be calculated:

$$S_{sp} = \frac{4}{\rho_f d}, \text{ provided that } d \ll a. \tag{7}$$

In the general case, $d \cong a$ and expression (7) becomes:

$$S_{sp} = \frac{4}{\rho_f} \left(\frac{1}{a} + \frac{1}{d}\right). \tag{7'}$$

Equation (5) establishes the relationship between the specific surface area and the average size of nanofibrils in NOA materials, which is consistent with the experimental results within 5% accuracy. Equation (7) was used to describe the evolution of aspect ratio a/d in the entire temperature range. Evolution of the mean diameter $d(T)$ of NOA fibrils calculated from (7) using fibril's density $\rho_f(T)$ and specific surface area $S_{sp}(T)$ obtained from isochronous annealing data is presented in Fig. 7. One more expression relating the specific density and specific surface area in NOA materials can be obtained from (2) and (7):

$$\rho \cdot S_{sp} = \pi \cdot n_f \frac{d}{a^2}, \text{ or } \rho \cdot S_{sp} \cdot \delta \approx 1, \text{ where } \delta = \frac{1}{\pi \cdot n_f} \cdot \frac{a^2}{d}. \tag{8}$$

Taking into account the limited range of n_f variation, the estimate of the "effective size of NOA fibril" can be obtained as $\delta \approx 0.02(a^2 d)$.

We notice that the mean fibril diameter observed in TEM images of raw NOA (Fig. 1b) is about 5 nm, that

fits the value obtained from (7) using the initial mass density 0.025 g/cm^3 and specific area $320 \text{ m}^2/\text{g}$. The similar estimations of the effective diameter of nanofibrils result in values about 7 nm in γ -alumina ($\rho = 0.04 \text{ g/cm}^3$, $S_{sp} = 150 \text{ m}^2/\text{g}$), 9 nm in θ -alumina ($\rho = 0.045 \text{ g/cm}^3$, $S_{sp} = 100 \text{ m}^2/\text{g}$) and 120 nm in α -phase ($\rho = 0.65 \text{ g/cm}^3$, $S_{sp} = 5 \text{ m}^2/\text{g}$) which are in agreement with the TEM and SEM observations. We conclude that the model proposed successfully describes 3D transformations in NOA materials during thermal treatment.

Evolution of the morphology of NOA fibrils under annealing

Three main temperature regions that change the mass transfer mechanism and activation of sintering process in NOA materials should be highlighted.

Low annealing temperatures $T < 300 \text{ }^\circ\text{C}$ In this temperature range, the structure of the raw $\text{Al}_2\text{O}_3 \cdot n\text{H}_2\text{O}$ material is preserved in the fibrils and the changes of the shape or in aspect ratio are small. Changes in the material density also can be neglected despite the fact that the value of $n(T)$ varies between 3.6 and 1.5 (Figs. 3 and 4, Table 2). We assume that water losses do not lead to any significant modification of the material morphology at nano- and micro-level.

Moderate annealing temperatures $T \leq 870 \text{ }^\circ\text{C}$ The NOA density changes upon annealing in this temperature range are below 0.01 g/cm^3 . We assume that the shape modifications of amorphous fibrils are limited by

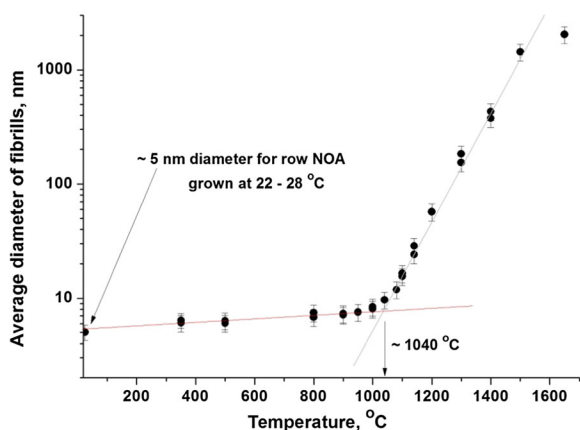


Fig. 7 Mean diameter of NOA fibrils, estimated from (7), versus temperature of isochronous annealing during 4 h

the diffusion transport and takes place at the fibril surface. This process leads to a decrease in the surface-to-volume ratio. Since both agglomeration and sintering of fibrils are not observed under these conditions, we can express the reduction in fibril length $a(t)$ and increase in its diameter $d(t)$ simply as a result of surface diffusion. We assumed that:

$$a(t) = a_0 - \sqrt{Dt}, \tag{9}$$

where a_0 is the initial fibril length and D is “efficient diffusion coefficient” which is related mostly to the surface. We also neglect mass transport between fibrils and consider the modification of a single fibril. On the basis of conservation of the fibrils volume, we can write:

$$d^2(t) = d_0^2 \frac{a_0}{a_0 - \sqrt{Dt}}. \tag{10}$$

From (9) and (10), one can obtain the shape variation of the fibril during annealing:

$$\frac{a}{d}(t) = \frac{a_0}{d_0} \left(1 - \frac{\sqrt{Dt}}{a_0} \right)^{\frac{3}{2}}, \tag{11}$$

where $D = D_0 \cdot \exp\left(-\frac{E_a}{k_B T}\right)$ is the “effective” diffusion coefficient with an activation energy E_a . Using (2), (7), (10), and (11), we can describe the changes in density and specific surface area of NOA materials at temperatures below $870 \text{ }^\circ\text{C}$:

$$\rho(t) = \rho_f n \frac{\pi}{4} \frac{\left(\frac{d_0}{a_0}\right)^2}{\left(1 - \frac{\sqrt{Dt}}{a_0}\right)^3} \tag{12}$$

$$S_{sp}(t) = \frac{4}{\rho_f} \left(\frac{1}{a(t)} + \frac{1}{d(t)} \right) = \frac{4}{\rho_f} \left(\frac{1}{a_0 \left(1 - \frac{\sqrt{Dt}}{a_0}\right)} + \frac{\sqrt{\left(1 - \frac{\sqrt{Dt}}{a_0}\right)}}{d_0} \right) \tag{13}$$

The “effective” diffusion coefficient: $D_0 = 6.0 \times 10^{-18} \text{ m}^2/\text{s}$ and activation energy $E_a = 28 \text{ kJ/mol}$ were estimated by applying the least-squares fit to the all experimental data for $\rho(t)$ and $S_{sp}(t)$ with the set of parameters: $a_0 = 140 \text{ nm}$, $d_0 = 5 \text{ nm}$, $\rho_f = 3.1 \text{ g/cm}^3$. Figure 8 show a good agreement between the experimental data and the model plot for a/d . The value of activation energy E_a is close to the activation energy of oxyhydroxide decomposition $E_D = 22 \pm 5 \text{ kJ/mol}$

obtained from TG data. Therefore, we assume that surface diffusion and chemical decomposition of the oxyhydroxide are intrinsically connected and possess a common activation mechanism for these processes.

The applied formalism is relevant to the conditions when the diffusion mass transport is limited within a single fibril: $a_0 \geq \sqrt{Dt}$. The single fibril of raw NOA has the mean volume $V_f \approx (2.5\text{--}3.0) \times 10^3 \text{ nm}^3$ and cylindrical shape with the aspect ratio $a/d \approx 30$. The surface mass transport results in the shape changes described by Eqs. (9)–(11). Consequently, the aspect ratio decreases by minimizing the surface energy reaching a minimum when $a/d \rightarrow 1$ and $l_{\max}(a_x \approx d_x) \approx 15 \text{ nm}$, but it does not take place due to diffusion limitations at temperatures below $870 \text{ }^\circ\text{C}$ and the aspect ratio remains larger than 20 (Fig. 8).

Thus, at moderate temperatures $\leq 870 \text{ }^\circ\text{C}$ with the short annealing times $\leq 10 \text{ h}$, when high porosity is remaining, the parameters of mesoporous NOA materials such as specific surface area, density, porosity, evolution of fibrils shape, and aspect ratio can be described using Eqs. (11–13).

High annealing temperatures $T \geq 870 \text{ }^\circ\text{C}$ An annealing of the NOA materials at temperatures higher $870 \text{ }^\circ\text{C}$ leads to significant coarsening of the alumina particles and those attains the sizes of $100\text{--}500 \text{ nm}$ that is much larger than the maximum estimates $\sim 10 \text{ nm}$ for the average size of the fibril in raw NOA. The mass transport progressively involves the overall volume of fibrils and the area of contacts between adjacent fibrils. The annealing at temperatures above $1000 \text{ }^\circ\text{C}$ leads to a significant shrinkage of NOA materials, which is related to an increase in the samples density and decrease in free volume. The initial porosity of raw NOA sample is $\geq 99\%$ and only slightly decreases to 98.8% after 4 h annealing at $1000 \text{ }^\circ\text{C}$. Further increase in the temperature results in a sharp decrease in porosity down to 71% at $1400 \text{ }^\circ\text{C}$, 56% at $1500 \text{ }^\circ\text{C}$, and to 26% at $1650 \text{ }^\circ\text{C}$. It is important to notice significant changes in the fibril morphology, which becomes spherical or ellipsoidal with the aspect ratio $(a/d) \leq 2$.

The structural evolution of NOA materials at high temperatures was described using a simplified version of Ivensen equation (Ivensen 1995). We assume that the changes of free volume in time follow the relationship:

$$\frac{dV}{dt} = -BV, \text{ where } B = B_0 \cdot \exp\left(-\frac{E_b}{RT}\right), \quad (14)$$

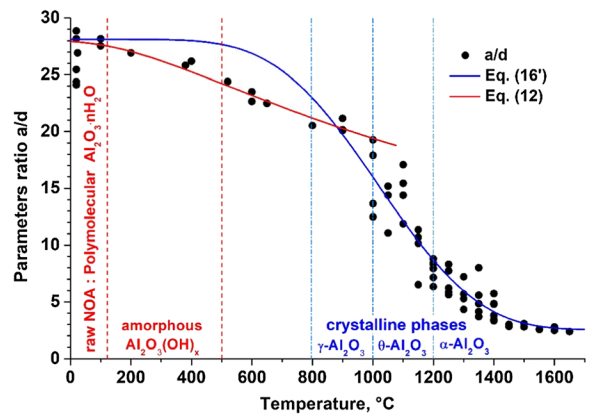


Fig. 8 Evolution of NOA fibrils aspect ratio a/d of NOA with annealing temperature. The results obtained both in this work and published earlier (Vignes et al. 1997; Di Costanzo et al. 2004; Vignes et al. 2008; Askhadullin et al. 2008) are presented. The scatter of the a/d ratio near the temperature $\sim 20\text{--}25 \text{ }^\circ\text{C}$ are caused by variation of humidity and air temperature during the measurements of raw NOA samples

and V is a free space (volume) between the fibrils. Coefficient B comprises two constants: the activation energy of the mass transport E_b , and the constant of free volume B_0 . The solution of Eq. (14) allows obtaining the dependence of free volume $V_{\text{free}}(t, T)$ from the sintering temperature T and time t :

$$V_{\text{free}}(t, T) = V_0 \exp\left(-B_0 t \cdot \exp\left(-\frac{E_b}{RT}\right)\right), \quad (15)$$

where V_0 is the free volume in NOA sample at $t = 0$. It is easy to get similar relationship for the NOA density $\rho(t, T)$:

$$\rho(t, T) = \frac{\rho_f V_f}{V_f + V_{\text{free}}(t, T)} = \frac{\rho_f}{1 + \frac{V_{\text{free}}(t, T)}{V_f}}, \quad (16)$$

From (16), we can define the initial density of NOA at $t = 0$, and from (16) we can define the initial density of NOA at $t = 0$ as $\rho_0 = \rho_f / (1 + V_0 \cdot V_f^{-1}) \approx (\rho_f V_f) / V_0$, and in combination with expression (15), we get:

$$\rho(t, T) = \frac{\rho_f}{1 + \frac{\rho_f}{\rho_0} \exp\left(-B_0 t \cdot \exp\left(-\frac{E_b}{RT}\right)\right)}. \quad (16')$$

From the definition of n_f can be obtained the relationship:

$$\rho_0 \left(\frac{a_0}{d_0}\right)^2 = \rho(t, T) \left(\frac{a}{d}\right)^2, \quad (4')$$

and after some transformations and substitutions in (16), we get the function describing an aspect ratio a/d evolution during sintering of NOA materials:

$$\begin{aligned} \frac{a}{d}(t, T) &= \frac{a_0}{d_0} \sqrt{\frac{\rho_0}{\rho(t, T)}} \\ &= \frac{a_0}{d_0} \sqrt{\frac{\rho_0 + \rho_f \exp\left(-B_0 t \cdot \exp\left(-\frac{E_b}{RT}\right)\right)}{\rho_f}} \approx \frac{a_0}{d_0} \exp\left(-\frac{B_0 t}{2} \cdot \exp\left(-\frac{E_b}{RT}\right)\right) \end{aligned} \quad (17)$$

The latter expression was obtained assuming that $\rho_f \gg \rho_0$.

After applying the least-squares fit to the experimental data shown in Fig. 8, the following values of the parameters in Eqs. (16') and (17) were obtained: $\rho_f = 3.1 \text{ g/cm}^3$, $B_0 = 2.3 \times 10^{-2} \text{ s}^{-1}$, and $E_b = 61 \text{ kJ/mol}$. The determined parameters B_0 and E_b were used for a/d and $\rho(t, T)$ curve plotting shown in Figs. 8 and 9. Obviously, that Eqs. (16') and (17) describe fairly well the results obtained for NOA samples after annealing at the temperatures $T \geq 870 \text{ }^\circ\text{C}$.

A characteristic feature of this temperature range is the process of sintering covering the whole volume and contact areas of the adjacent nanofibrils, which is accompanied by profound restructuring of the mesoporosity as well as with the processes of crystallization and phase transformations. Since the $\gamma \rightarrow \theta \rightarrow \alpha$ phase transformations are characterized by very close values of the activation energy E_b , the relevant process can be considered as permanent and progressive ordering in the crystalline structure due to release of residual

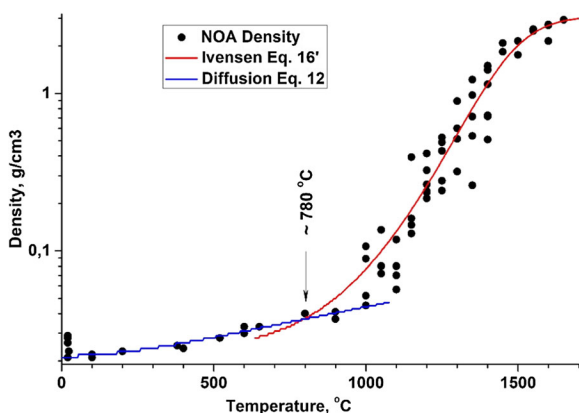


Fig. 9 The application of the model to describe changes in the mass density of NOA samples in the temperature range ~ 20 – $1700 \text{ }^\circ\text{C}$. Equation (12) was applied to the density data in the range $T \leq 1000 \text{ }^\circ\text{C}$ (blue line) and Iverson's simplified Eq. (16') was used for the temperatures $T \geq 800 \text{ }^\circ\text{C}$ (red line)

structural water from the fibrils. A complete water removal from the NOA structure takes place at the formation of the α -phase. The activation energy of the sintering $E_b = 61 \text{ kJ/mol}$ is considerably higher than $E_a = 28 \text{ kJ/mol}$ —the assessment made for moderate annealing temperatures $T \leq 870 \text{ }^\circ\text{C}$ at which the changes of fibrils shape can be associated with the surface transport effects.

Conclusions

Chemical and structural modifications of mesoporous nanofibrous alumina $\text{Al}_2\text{O}_3 \cdot n\text{H}_2\text{O}$ were studied in the temperature range of 20 – $1700 \text{ }^\circ\text{C}$. Two mechanisms of the morphological and structural transformations in NOA materials are evidenced and the physical model was proposed allowing describing the changes in physical parameters such as density, porosity, and specific surface area as morphological evolution of the averaged structural element—the NOA fibril. At temperatures $< 300 \text{ }^\circ\text{C}$, the change in composition of amorphous $\text{Al}_2\text{O}_3 \cdot n\text{H}_2\text{O}$ is insignificant and is mainly due to desorption of molecular water; amorphous structure of raw NOA is preserved. At moderate temperatures between 300 and $870 \text{ }^\circ\text{C}$, the mass transport is limited by surface diffusion along the single fibrils and characterized by activation energy $E_a = 28 \text{ kJ/mol}$; this cause shrinkage of the fibril size about 20% and aspect ratio a/d decreasing from ~ 24 till 20 ; the onset of crystallization of amorphous NOA is not observed upon 4 h annealing. At high temperatures, the mass transport characterized by activation energy $E_a = 61 \text{ kJ/mol}$ and involves the overall volume of fibrils followed by the material sintering and growth of particles with the aspect ratio $a/d \leq 2$ and elliptical shape. The transition temperature from moderate to high temperatures is close to $870 \text{ }^\circ\text{C}$, which corresponds to the beginning of the crystallization of amorphous alumina to γ -phase. Applying 3D model for the experimental results analysis, we explain the phenomenon of preservation of the integrity of monoliths of NOA during thermal annealing by the important role of surface processes and first of all high mobility of atoms on the surface of nanofibrils. The surface diffusion provides an isotropic reduction in the 3D structure parameters without a significant increase in internal stresses over a wide range of temperatures. The model proposed allow a quantitative description of the morphological and structural properties of mesoporous

aluminas and may be useful for further development of the technology of 3D nanomaterials.

Acknowledgments ANR (Agence Nationale de la Recherche) and CGI (Commissariat à l'Investissement d'Avenir) are gratefully acknowledged for their financial support of this work through Labex SEAM (Science and Engineering for Advanced Materials and devices) ANR 11 LABX 086, ANR 11 IDEX 05 02.

Funding This work was supported by the French-Russian collaboration project DRI CNRS No. EDC26176, and part of this work was carried out with the financial support of the Russian Foundation for Basic Research (Project 17-53-150007 CNRS_a).

Compliance with ethical standards

Conflict of interest The authors declare that they have no conflict of interest.

References

- Asadchikov VE, Askhadullin RS, Volkov VV, Dmitriev VV, Kitaeva NK, Martynov PN, Osipov AA, Senin AA, Soldatov AA, Chekrygina DI, Yudin AN (2015) Structure and properties of “nematically ordered” aerogels. *JETP Lett* 101:556–561. <https://doi.org/10.1134/S0021364015080020>
- Askhadullin RS, Martynov PN, Yudintsev PA, Simakov AA, Chaban AY, Matchula EA, Osipov AA (2008) Liquid metal based technology of synthesis of nanostructured materials (by the example of oxides). These materials properties and applications areas. *J Phys: Conf Ser* 98:1–6. <https://doi.org/10.1088/1742-6596/98/7/072012>
- Bouslama M, Amamra MC, Tieng S, Brinza O, Chhor K, Abderrabba M, Vignes JL, Kanaev A (2011) Isolation of titania nanoparticles in monolithic ultraporous alumina: effect of nanoparticle aggregation on anatase phase stability and photocatalytic activity. *Appl Catal A* 402:156–161
- Bouslama M, Amamra MC, Jia Z, Ben Amar M, Brinza O, Chhor K, Abderrabba M, Vignes JL, Kanaev A (2012) Nanoparticulate TiO₂-Al₂O₃ photocatalytic media: Effect of particle size and polymorphism on photocatalytic activity. *ASC Catal* 2:1884–1892
- Di Costanzo T, Fomkin AA, Frappart C, Khodan AN, Kuznetsov DG, Mazerolles L, Michel D, Minaev AA, Sinitsin VA, Vignes JL (2004) New method of porous oxide synthesis: alumina and alumina based compounds. *Mater Sci Forum* 453-454:315–322
- Frappart C (2000) Elaboration et caractérisation de monolithes poreux d'alumine obtenus par oxydation d'aluminium. Insertion d'oxydes nanométriques, PhD Dissertation, University Paris 11
- Ivensen VA (1995) Use of a mathematical model for pore volume shrinkage over a wide temperature range. *Powder Metall Met Ceram* 34:528–533. <https://doi.org/10.1007/BF00559962>
- Khatim O, Amamra M, Chhor K, Bell T, Novikov D, Vrel D, Kanaev A (2013) Amorphous-anatase phase transition in single immobilised TiO₂ nanoparticles. *Chem Phys Lett* 558:53–56
- Khodan AN, Kopitsa GP, Yorov KE, Baranchikov AE, Ivanov VK, Feoktystov A, Pipich V (2018) Structural analysis of aluminum oxyhydroxide aerogel by small angle X-ray scattering. *J SURF INVESTIG-X-RA* 12:287–296
- McHale JM, Auroux A, Perrotta AJ, Navrotsky A (1997a) Surface energies and thermodynamic phase stability in nanocrystalline aluminas. *Science* 277:788–791
- McHale JM, Navrotsky A, Perrotta AJ (1997b) Effects of increased surface area and chemisorbed H₂O on the relative stability of nanocrystalline γ -Al₂O₃ and α -Al₂O₃. *J Phys Chem B* 101:603–613
- Mukhin VI, Khodan AN, Nazarov MM, Shkurinov AP (2012) Study of the properties of nanostructured aluminum oxyhydroxide in the terahertz frequency range. *Radiophys Quant Electron* 54:591–599
- Navrotsky A (2003) Energetics of nanoparticle oxides: interplay between surface energy and polymorphism. *Geochem Trans* 4:34–37
- Noordin MR, Liew KY (2010) Synthesis of alumina nanofibers and composites, in: Kumar A (ed.) *Nanofibers*, InTech
- Pinnel MR, Bennett JE (1972) Voluminous oxidation of aluminium by continuous dissolution in a wetting mercury film. *J Mater Sci* 7:1016–1026
- Stepanenko O, Tartari A, Amamra M, Nguyen THN, Piat M, Favero I, Ducci S, Khodan A, Boinovich LB, Emelyanenko AM, Kanaev A, Leo G (2015) Ultra-porous alumina for microwave planar antennas. *Adv Device Mater* 1:93–99. <https://doi.org/10.1080/20550308.2015.1120442>
- Vignes JL, Mazerolle L, Michel D (1997) A novel method for preparing porous alumina objects. *Key Eng Mater* 132-136: 432–435
- Vignes JL, Frappart C, Di Costanzo T, Rouchaud JC, Mazerolles L, Michel D (2008) Ultraporous monoliths of alumina prepared at room temperature by aluminium oxidation. *J Mater Sci* 43:1234–1240
- Wislicenus H (1908) Über die faserähnliche gewässene Tonerde (Fasertonerde) und ihre Oberflächenwirkungen (Adsorption). *Zeitschrift für Chemie und Industrie der Kolloide* 2:XI-XX
- Zhang H, Banfield JF (1998) Thermodynamic analysis of phase stability of nanocrystalline titania. *J Mater Chem* 8:2073–2076